Modelling take-off moment arms in an ornithocheiraean pterosaur

Benjamin W Griffin [Corresp., 1, 2], **Elizabeth Martin-Silverstone** [1], **Rodrigo V Pêgas** [3], **Erik Anthony Meilak** [4], **Fabiana R Costa** [3], **Colin Palmer** [1], **Emily J Rayfield** [1]

[1] Palaeobiology Group, School of Earth Sciences, University of Bristol, Bristol, United Kingdom

[2] School of Biological and Environmental Sciences, Liverpool John Moores University, Liverpool, United Kingdom

[3] Laboratório de Paleontologia de Vertebrados e Comportamento Animal, Universidade Federal do ABC, Alameda da Universidade, s/n, Anchieta, 09606-045, São Bernardo do Campo, SP, Brazil

[4] School of Pharmacy and Bioengineering, University of Keele, Keele, United Kingdom

Corresponding Author: Benjamin W Griffin
Email address: b.w.griffin@ljmu.ac.uk

Take-off is a vital part of powered flight which likely constrains the size of birds, yet extinct pterosaurs are known to have reached far larger sizes. Three different hypothesised take-off motions (bipedal burst launching, bipedal countermotion launching, and quadrupedal launching) have been proposed as explanations for how pterosaurs became airborne and circumvented this proposed morphological limit. We have constructed a computational musculoskeletal model of a 5 m wingspan ornithocheiraean pterosaur, reconstructing thirty-four key muscles to estimate the muscle moment arms throughout the three hypothesised take-off motions. In all our models we found the muscles utilised in the quadrupedal take-off have the largest moment arms throughout the entire take-off sequences and for the take-off pose.

1 Modelling take-off moment arms in an

2 ornithocheiraean pterosaur.

3   B. W. Griffin[1], E. Martin-Silverstone[1], R. Pêgas[2], E. A. Meilak[3], F. Costa [2], C. Palmer[1], E. J.

4   Rayfield[1]

5   [1] Bristol Palaeobiology Group, School of Earth Sciences, University of Bristol, Life Sciences

6   Building, Bristol BS8 1TS, UK.

7   [2] Laboratório de Paleontologia de Vertebrados e Comportamento Animal, Universidade Federal

8   do ABC, Alameda da Universidade, s/n, Anchieta, 09606-045, São Bernardo do Campo, SP,

9   Brazil.

10   [3] School of Pharmacy and Bioengineering, University of Keele, Keele, United Kingdom

11

12 Abstract

13   Take-off is a vital part of powered flight which likely constrains the size of birds, yet

14   extinct pterosaurs are known to have reached far larger sizes. Three different hypothesised

15   take-off motions (bipedal burst launching, bipedal countermotion launching, and quadrupedal

16   launching) have been proposed as explanations for how pterosaurs became airborne and

17   circumvented this proposed morphological limit. We have constructed a computational

18   musculoskeletal model of a 5 m wingspan ornithocheiraean pterosaur, reconstructing thirty-four

19   key muscles to estimate the muscle moment arms throughout the three hypothesised take-off

20   motions. In all our models we found the muscles utilised in the quadrupedal take-off have the

21   largest moment arms throughout the entire take-off sequences and for the take-off pose.

22

23 **Introduction**

24   'Portions of this text were previously published as part of a thesis (https://research-

25   information.bris.ac.uk/ws/files/348718716/Final_Copy_2022_12_06_Griffin_B_W_PhD_Redacte

26   d.pdf)'.

27

28   Powered flight is a method of locomotion that is limited to very few animals as it is

29   energy intensive and requires specific adaptations to achieve launch, as well as deriving thrust

30   and weight support via lift (Rayner, 1989). The most power-intensive part of powered flight is

31   take-off from the ground. This stage requires the animal to get high enough into the air to utilise

32   an unobstructed flapping cycle. Take-off also requires the animal to generate enough velocity

33   such that the wings produce enough lift to overcome drag (e.g. thrust) and support the weight of

34   the animal (Pennycuick, 1968; Rayner, 1988; Alexander, 1998). The height and velocity

35   requirements both increase with larger size, making take-off size-limiting for flying animals. No

36   modern flying animal exceeds a mass of 25kg with the heaviest volant living animal, *Otis tarda*

37   (the Great Bustard), recorded as reaching 22kg (Henderson, 2010). This limit has been

38   previously attributed to the differential in scaling between increases in mass and increases in

39   available muscle power which is predicted to increase at approximately mass$^{0.75}$ (Alexander,

40   1998). Despite this, many extinct animals have reached greater sizes and are still considered

41   capable of flight, including birds such as *Argentavis magnificens* and *Pelagornis sandersi* which

42   are predicted to have masses of 70kg and 21.8-40kg respectively (Goto et al., 2022).

43   Pterosaurs vary in size, with medium sized pterosaurs reaching wingspans between 2 and 5m

44   predicted and masses ranging between 2kg to 30kg (Witton, 2008; Martin-Silverstone, 2017;

45   Goto et al., 2022). Pterosaurs have also reached the largest sizes of any animal considered

46   volant with the largest pterosaurs such as *Quetzalcoatlus northropi* predicted to have reached

47   much greater masses (150kg, or more commonly 250kg (Witton, 2008; Witton & Habib, 2010;

48   Padian et al., 2021)). Flight at such large body masses challenges our understanding of the

49   functional limits of flight making understanding take-off in pterosaurs crucial to establishing the

50   functional limits of flight in organisms.

51   There are two main hypotheses for how pterosaurs launched. The bipedal launch

52   hypothesis is based on modern bird take-offs while the quadrupedal launch hypothesis is

53   partially inspired by vampire bat take-offs (Habib, 2008). For an unassisted bipedal take-off,

54   birds broadly fall into two different motions (Earls, 2000). In the first style, hereafter referred to

55   as the bipedal countermotion take-off, the animal starts in a terrestrial locomotory bipedal pose.

56   As the take-off cycle starts, the animal begins a crouching counter movement where it bends its

57   hindlimbs and lowers its centre of mass while beginning to lean forward. The animal then rapidly

58   extends the wings and hind limbs to launch, pushing the animal forward and upward. This take-

59   off style is more favoured by birds that are less specialised for terrestrial locomotion, for

60   example the European starling *Sturnis vulgaris* (Earls, 2000).

61   The second take-off motion is hereafter referred to as a bipedal burst take-off. This take-

62   off begins already in a deep crouch and then rapidly extends the hind limbs with the body

63   angled to launch nearly vertically while the wings start their initial downstroke. Because of the

64   near vertical launch trajectory this take-off style results in limited forward motion but reaches

65   greater heights. This style of take-off is favoured by birds that are specialised for living primarily

66   terrestrially and fly rarely such as the European migratory quail *Coturnix coturnix* (Earls, 2000).

67   A proposed mode of take-off was recently proposed for the largest pterosaurs (Padian et al.,

68   2021) which is nearly identical to the bipedal burst take-off. The only substantial difference

69   between the bipedal burst take-off of birds and proposed pterosaur take-off is that pterosaurs

70   could not start to utilise the wings to assist with the take-off until a sufficient height is reached for

71   the wings to clear the ground. The distal wings of pterosaurs were unable to deform in the same

72   manner as the feathers of a bird due to the bony spar that supports the pterosaur wing

73   membrane so any contact with the ground during flapping would have likely damaged the wing

74   (Hone, Van Rooijen & Habib, 2015). As this is the only distinction, we consider this model of

75   pterosaur take-off as a bipedal burst take-off in our analysis.

76   The quadrupedal launch hypothesis described for pterosaurs is split into three main

77   steps starting from a quadrupedal stance (Habib, 2008; Molnar, 2009; Griffin et al., 2022). The

78   first is a crouching counter movement much like the bipedal take-off. When the deepest part of

79   the crouch was reached the pterosaur began extending its hindlimbs providing an initial forward

80   impulse and pushing the pterosaur onto its forelimbs. When the hindlimbs leave the ground the

81   vault phase began. During this phase, the hindlimbs assumed the pose utilised in flight and the

82   weight of the animal shifted to be entirely supported by the forelimbs. The launch phase then

83   started as the forelimbs began to extend, pushing the pterosaur upwards and forwards until the

84   forelimbs lost contact with the ground. This differs from a standard vampire bat take-off where

85   the take-off is almost vertical; in vampire bats the launch impulse is generated almost entirely by

86   the forelimbs (Schutt Jr. et al., 1997) instead of both the forelimbs and the hindlimbs in

87   pterosaurs (Habib, 2008; Witton, 2013).

88   While the difference in the structural strength of pterosaur forelimb and hindlimb bones

89   led to the original proposal of the quadrupedal take-off (Habib, 2008) and a recent study

90   quantitatively investigated quadrupedal water take-off (Pittman et al., 2022), there has been

91   very limited quantitative testing of the terrestrial take-off published (Padian et al., 2021; Griffin et

92   al., 2022). Particularly of note, the ability of these take-off motions to generate the leverage that

93   would be necessary to propel large pterosaurs into the air has not been quantitatively tested.

94   One method for assessing leverage in extinct animals is the calculation of muscle moment arms

95   (Hutchinson et al., 2005; Bates et al., 2012; Maidment, Bates & Barrett, 2014; Allen, Kilbourne &

96   Hutchinson, 2021; Bishop, Cuff & Hutchinson, 2021). While muscle lines of action have been

97   presented previously for pterosaurs (Fastnacht, 2005; Costa, Rocha-Barbosa & Kellner, 2014) these

98   studies focussed primarily on myological reconstruction for terrestrial locomotion and did not

99   calculate the moment arms.

100   To test the ability of different pterosaur take-off hypotheses to produce leverage during

101   the launch phase we have constructed the first OpenSim musculoskeletal model pterosaur. This

102   model is based on a 5 m wingspan ornithocheiraean pterosaur. Using this model, we have

103   estimated the take-off applicable muscle moment arms around each joint throughout the take-off

104   motions for each of the hypothesised take-offs. Moment arm estimations serve as the first step

105   in more complicated estimations of moment and power generation through take-off. However,

106   we hypothesise that the leverage of the hindlimbs during the launch phase would be greatest in

107   the bipedal burst followed by the countermotion motions, as these motions rely on the leverage

108   of the hindlimbs to power a bipedal take-off (Meilak et al., 2021a), while the leverage of the

109   forelimbs will be greater in the quadrupedal launch phase than either of the bipedal take-offs.

110

Materials & Methods

111

OpenSim modelling.

112

113   An ornithocheiraean musculoskeletal model was constructed using µCT scans of SMNK-

114   PAL 1133, an indeterminate ornithocheiraean pterosaur. The OpenSim model was based upon

115   a skeletal model made in Maya for a different study in 2015 (Martin-Silverstone, 2017; Martin-

116   Silverstone, Sykes & Naish, 2018; Griffin et al., 2022). This specimen was selected due to the 3D

117   preservation of the skeletal elements and relative completeness of the specimen. Further as a

118   medium sized 5m wingspan pterosaur the ability to successfully take-off can be more readily

119   assumed than for the giant 10m wingspan pterosaurs. The surface meshes from the skeletal

120   model were checked and any errors were cleaned using Geomagic Studio (3Dsystems,

121   Morrisville, NC, USA). The articulated OpenSim model was constructed utilising the cleaned

122 surface meshes and fitted geometric shapes following the workflow of Meilak *et al.* (2021a)

123 using MATLAB v2021a, ParaView v5.9.0-RC3 (Ahrens, Geveci & Law, 2004), and OpenSim v4.0

124 and v4.1 (Seth et al., 2018). Due to the incomplete nature of SMNK-PAL 1133 scaled cylinders

125 were added to represent the tibia and wing phalanges III and IV while duplicates of existing

126 elements were used for missing vertebrae. The anterior skull is a scaled version of AMNH

127 FARB 24444 combined with the anterior section of SMNK 1133 (Griffin et al., 2022).

128   The joints of the articulated OpenSim model each include three rotational degrees of

129 freedom (DOF). The individual DOF axes are aligned with specific movements of the limbs

130 following the same definitions as Kambic *et al.* (2014). Rotation along the abduction/adduction

131 axis degree of freedom results in the limb moving away/towards the midline of the body.

132 Flexion/extension axis rotation results in decreasing/increasing angles between the limbs. While

133 long axis rotation along the axis rotates the distal element along the longest axis of the element.

134 Not all DOFs included within the model are informative for take-off however all three DOFs in

135 the shoulder and hip along with the flexion/extension DOF in the elbow, wrist, wing metacarpal,

136 first wing phalanx, and knee are all expected to contribute to the take-off motion (Figures 1, 2).

137 **Muscle Geometry.**

138   Twenty-two muscles related to forelimb motion and a further twelve muscles related to

139 the movement of the hip and knee joints were modelled as muscle tendon units (MTUs) in the

140 OpenSim model following the estimated lines of action between the origin and insertion points

141 (Table 1 including abbreviations, Figure 1). The MTUs were modelled based upon examination

142 of physical specimens (Supplementary Material) and muscle reconstructions in the literature

143 (Dilkes, 1999; Bennett, 2001a,b, 2003, 2008; Fastnacht, 2005; Molnar, 2009; Witton, 2013; Costa, Rocha-

144 Barbosa & Kellner, 2014; Tokita, 2015; Frigot, 2017). For completeness, every muscle predicted to

145 be involved in the take-off by these prior literature reconstructions (Bennett, 2001a, 2003, 2008;

146 Fastnacht, 2005; Molnar, 2009; Witton, 2013; Costa, Rocha-Barbosa & Kellner, 2014; Tokita, 2015;

147 Frigot, 2017) were included in our model. Inference levels for the presence of each muscle were

148 determined following the extant phylogenetic bracket (EPB) inference model of Witmer (1995)

149 and recorded in Table 1. Pterosaurs are bracketed by crocodiles and birds, following the most

150 accepted interpretation of Pterosauromorpha as the sister-group of the Dinosauromorpha within

151 Archosauria (Ezcurra et al., 2020; Baron, 2021; Foffa et al., 2022; Kellner et al., 2022). Muscles

152 were only modelled when the inferred levels of confidence (as established by Witmer (1995)) for

153 their origin and insertion were assessed as either I or II (positive or equivocal assessment,

154 respectively). Whenever direct correlates in the form of osteological markers could not be

155 identified, apostrophes (as in I' and II') indicate that correlates were missing, but reconstruction

156 is still carried out based on the myological patterns present in the phylogenetic bracketing

157 groups. Supplementary Table 1 summarizes all areas of origin and insertion, as well as their

158 respective correlates (when present) and inference levels, for each reconstructed muscle. In the

159 model, each origin and insertion point were placed at the centroids of the inferred areas of

160 attachment with interpenetration between the bone meshes and the MTUs controlled by via

161 points and wrapping surfaces (Hutchinson et al., 2015; Modenese & Kohout, 2020; Bishop, Cuff &

162 Hutchinson, 2021; Meilak et al., 2021a; Wiseman et al., 2021).

163   To portray the complex lines of action more accurately in muscles with multiple origins

164 such as the *m. triceps* and the *m. flexor tibialis internus* each muscle head was modelled

165 individually (Table 1). For large muscles with broad attachment areas multiple lines of action

166 were modelled at the cranial and caudal extents of the muscle in addition to a central muscle

167 line of action. For the *m. pectoralis* lines of action were modelled at the cranial, caudal, medial,

168 and lateral origin extent instead of a central muscle line of action, to better capture the broad

169 origin and insertion of the muscle. The line of action moment arms were then averaged for these

170 large muscles and this average value was used for examination of summed moment arms. In

171   total, the present model includes 36 MTUs pertaining to wing musculature, and 18 MTUs related

172   to the hip and knee musculature (Table 1).

173   **Kinematics.**

174   Key poses from the literature (Bramwell & Whitfield, 1974; Padian, 1983; Fastnacht, 2005;

175   Molnar, 2009; Chatterjee & Templin, 2012; Witton, 2013; Costa, Rocha-Barbosa & Kellner, 2014; Padian

176   et al., 2021) for the hypothesised take-offs were created for the OpenSim model and corrected to

177   fit within the range of motion calculated for the model via a previous study using the ROM

178   mapping methodology (Griffin et al., 2022). Intermediate poses were extrapolated using inverse

179   kinematics in Maya and OpenSim to create a full kinematic profile of each take-off (Figure 3).

180   The timing between each pose was determined by relating the timing of each key pose of the

181   model take-off sequences with the timing of the equivalent pose in the extant take-off

182   sequences for the different take-off styles (Schutt Jr. et al., 1997; Earls, 2000). The total time of

183   the entire model sequence was then normalised as one second take-off motions. Directionality

184   of joints are shown in Figure 2.

185   The bipedal burst take-off timings are based on a quail profile (Earls, 2000) and the

186   description by Padian *et al.* (2021). The take-off has been split into three phases (Figure 3A)

187   starting with the crouch phase which begins in the fully crouched pose and lasts until the ankle

188   joint loses contact with the ground. From this point the second phase, termed the ankle lifted

189   phase, contains the continued leg extension, finishing when the pterosaur reaches a fully

190   digitigrade pose. The final phase is the launch phase where the leg extension moves the

191   pterosaur from the digitigrade pose to the point where the feet lose contact with the ground and

192   the wing moves to the start of the flight downstroke position.

193   The bipedal countermotion timings are based on a starling profile (Earls, 2000) and the

194   earlier descriptions of pterosaur bipedal take-off poses (Padian, 1983; Chatterjee & Templin, 2004,

195   2012; Fastnacht, 2005). The take-off has been split into two phases (Figure 3B). The first phase is

196   termed the countermotion phase and contains the starting bipedal stance through the flexion of

197   the hindlimb and the unfurling of the wing. The second phase is the launch phase and includes

198   the extension of the hindlimb and movement of the wing into the start of the flight downstroke

199   position.

200   The quadrupedal take-off timing is based on a vampire bat profile (Schutt Jr. et al., 1997)

201   and primarily follows the description by Habib (2008) modified by other descriptions of key

202   poses in the literature (Fastnacht, 2005; Molnar, 2009; Witton, 2013). The quadrupedal take-off

203   has been split into three phases (Figure 3C). The first phase is termed the crouch phase which

204   begins in a quadrupedal stance pose and continues until the hindlimbs and forelimbs are fully

205   flexed. The vault phase then includes the extension of the hindlimbs as the pterosaur pushes

206   itself fully onto the forelimbs. The final phase is the launch, wherein the forelimbs extend until

207   they leave the ground and the hindlimbs assume the pose that will be utilised in flight. As the bat

208   profile timing largely ignored the hindlimbs the timing of the hindlimb leaving the ground in the

209   vault phase was added using the timing of the literature descriptions of the pterosaur

210   quadrupedal take-off (Habib, 2008; Molnar, 2009) relative to the timing of this phase for the

211   forelimbs.

212   **Moment Arm analysis.**

213   Moment arms were recorded for each pose throughout the take-off kinematics in the shoulder,

214   elbow, wrist, wing metacarpal, and wing phalanx 1 in the forelimb and the hip and the knee in

215   the hindlimb. These joints were selected as they are the joints proposed to be utilised in the

216   different launch hypotheses. The ankle joint was not included due to the lack of an accurate

217   bone models of the tibia and metatarsals, preventing accurate mapping of the MTUs which adds

218   a large amount of error to moment arm estimations (Meilak et al 2021a). Moment arms were

219   calculated and exported using the plotting tool in OpenSim for the kinematic sequence of each

220 take-off in each joint degree of freedom (DOF). OpenSim calculates moment arms using the in-

221 built the virtual work methodology (An et al., 1984; Pandy, 1999; Delp & Loan, 2000; Sherman, Seth &

222 Delp, 2013). Exported moment arms were then analysed using a modified R script (R version

223 4.1.2, Rstudio version 2021.09.2+382) based upon the methodology of Wiseman et al.

224 (Wiseman et al., 2021). As in the Wiseman methodology a Monte Carlo simulation of each

225 muscle moment arm value was run wherein the value was independently allowed to uniformly

226 randomise by values of up to ± 20% for 1000 simulated trials to create error margins accounting

227 for errors in moment arm estimation. The resultant distribution was then analysed for both the

228 mean moment arm and the standard deviation. The mean moment arms for each muscle were

229 collated to determine the total summed moment arms and overall direction of the moment arm

230 acting upon the joint at each point in the launch hypothesis motions.

231 ## Results

232 The following results apply the summed directional moment arms and associated

233 estimation error calculated from the Monte Carlo approach plotted against the launch kinematics

234 (Figures 3-5). Trends applicable to launch are summarised below.

235 ***Bipedal Burst.***

236 The hip abductors through the bipedal burst kinematic initially decrease before

237 plateauing in the ankle lifted phase of the take-off. The adductors show a steady increase

238 through the entire kinematic. With regards to rotation the internal rotators of the hip decrease

239 through the entire take-off sequence while the extensors only begin to increase noticeably

240 during the ankle lifted phase. The flexor moment arms in the hip slightly increase through the

241 entire take-off kinematic as do the hip and knee extensors. The knee flexors also sharply

242 increase during the crouched phase before beginning to slow during the ankle lifted phase.

243   ***Bipedal Countermotion.***

244   For the bipedal countermotion kinematic the moment arms of the hip abductors show an

245   increase through the countermotion before decreasing in the launch phase. The adductors show

246   a slight decrease during the countermotion phase, increase slightly at the start of the launch

247   phase before ultimately decreasing further. Regarding hip rotational moment arms the internal

248   rotators are largely unchanged through the countermotion phase and then increase slightly

249   during the launch phase. The external rotator moment arms decrease throughout the

250   countermotion phase and then increase through the launch phase. For the flexor moment arms

251   there is a decrease through the countermotion phase and in increase through the launch phase.

252   This pattern is repeated in the hip extensor moment arms until midway through the launch

253   phase where the length of the moment arms begins to decrease again. The knee flexor moment

254   arms increase through the countermotion phase and decrease through the launch phase while

255   the knee extensor moment arms remain largely unchanged throughout the take-off kinematic.

256   ***Quadrupedal.***

257   Shoulder abductors through the quadrupedal take-off kinematic remain largely

258   equivalent until the launch phase where they see a decrease in leverage, conversely the hip

259   abductors increase until the hindlimbs leave the ground in the vault phase. The shoulder

260   adductors show an increasing trend until the launch phase where it sharply decreases while the

261   hip adductors decrease until the vault phase. The shoulder internal rotation DOF moment arms

262   increase through the crouch phase and decrease through the rest of the take-off kinematic while

263   the external rotation DOF shows the reverse. The hip internal rotators feature a decrease in the

264   middle of the crouch phase but are otherwise largely unchanged. The external rotators on the

265   other hand feature a pronounced decrease through the crouch phase.

266   The shoulder flexion moment arms decrease through the crouch phase before

267   increasing slowly in the vault and rapidly in the launch phase. The extensor moment arms

268   slightly increase throughout the kinematic until the launch phase where they rapidly decrease.

269   The elbow flexors slightly decrease through the crouch phase. This decrease becomes more

270   pronounced in the vault phase and reverses in the launch phase. The extensor moment arms

271   slightly increase throughout the crouch and vault phases before decreasing during the launch

272   phase. The wrist flexion moment arms increase during the crouch phase and then decrease

273   through the rest of the take-off while the extensor moment arms are largely unchanged through

274   the kinematic sequence. The wing metacarpal (WMC) moment arm trends are equivalent to the

275   trends in the wrist however the WMC extension moment arms are half a large as the equivalent

276   wrist moment arms. The moment arms of the first wing phalanx (WP1) flexors are largely

277   consistent through the crouch phase before dipping slightly in the later phases of the take-off.

278   The extensors decrease until the end of the crouch phase and then increase again. In the

279   hindlimb, the hip flexors and extensors along with the knee extensors decrease through the

280   crouch phase while the knee flexors increase.

Discussion

282   The modelled launch motions include data for all of the muscles previous authors

283   (Bennett, 2001a, 2003, 2008; Fastnacht, 2005; Molnar, 2009; Witton, 2013; Costa, Rocha-Barbosa &

284   Kellner, 2014; Tokita, 2015; Frigot, 2017) have included in reconstructions of the fore and hind

285   limbs. It must be noted however that despite including the moment arms of the forelimbs in the

286   bipedal take-off models, the forelimbs would not be utilised at the point of take-off. In both

287   bipedal take-offs the forelimbs are not used until the initial downstroke of the wings by which

288   time launch has already occurred (Padian, 1983; Padian et al., 2021). Similarly, the

289   quadrupedal take-off does not utilise the hindlimb moment arms at the point of launch. The

290   quadrupedal take-off only utilises the hindlimbs until they lose contact with the ground during the

291   vault phase of the take-off (Habib, 2008). This limitation on the availability of leverage generated

292   by the launch underlies the hypothesis that the bipedal launches would generate a noticeable

293   increase in hindlimb moment arms during the launch phase and the quadrupedal would have

294   greater leverage in the forelimb. The results of our models (figures 4-6) do not find a large

295   increase in the leverage of the hindlimb in the bipedal take-offs relative to the quadrupedal take-

296   off. Conversely the quadrupedal take-off does provide greater moment arms in the forelimb than

297   the bipedal take-offs.

298   The largest moment arms that occur for each of the simulated take-offs occurs in the

299   upper forelimb joints, specifically in the elbow flexion/extension DOF and the shoulder

300   abduction/adduction DOF (Figure 4). The largest moment arms in the hindlimbs occur in each of

301   the hip DOFs and are largely equivalent between the different launches; except for the hip

302   external rotation DOF which has a smaller moment arm during the burst take-off (Figure 6).

303   Overall, the largest hindlimb moment arm is half the length of the largest forelimb moment arm.

304   The smallest moment arms occur in the extensional DOF of WP1 in the lower forelimb (Figure

305   5).

306   The largest summed moment arms are recorded in the forelimb for all three take-off

307   hypotheses, with the largest moment arms occurring in the quadrupedal take-off profile. Trends

308   within the take-off moment arms closely match phase changes within the different take-off

309   kinematics in all but the burst take-off hindlimb DOFs (Figure 6). There is distinct overlap in the

310   forelimb DOFs for the bipedal take-off motions which correspond with the wings gaining

311   sufficient clearance to fully open without striking the ground. Similarly, both the bipedal

312   countermotion and quadrupedal take-off hindlimb DOFs strongly overlap during the

313   countermotion phases of each take-off kinematic before diverging during the later phases. The

314   peak moment arms for the bipedal burst take-off tend to occur at launch or at the start of the

315   take-off sequence. The peak moment arms of the bipedal countermotion take-off tend to occur

316   during the countermotion phase or at launch except for the hip abduction and extension degrees

317   of freedom where the peak occurs at the start of the sequence. The quadrupedal take-off peak

318   moment arms occur at launch or the end of the crouch phase in the forelimb and at the end of

319   the crouch phase or start of the take-off sequence in the hindlimb, except for the hip long axis

320   rotation peak which occurs at launch as the hindlimbs assume the flight pose. Overall, when all

321   of the moment arms are considered, the quadrupedal take-off summed moment arms are

322   greater in magnitude than moment arms associated with the other two take-offs scenarios.

323   A complication in the muscular reconstruction process are the prominent differences

324   between crocodilian and avian estimations in the presence or absence of different muscles. The

325   TM, HR, FDL.U, and TR.M are absent in birds, and the TR.C is variable between species but

326   are all present in crocodilians; conversely the FCR is not present in crocodilians (Dilkes, 1999;

327   Bennett, 2003, 2008). The inclusion of these muscles results in changes to the muscle

328   reconstruction and the resultant moment arms of the model with entirely avian based moment

329   arms being slightly reduced compared to purely crocodilian or combined models (See

330   Supplementary). While it is possible to determine the presence of some muscles via muscle

331   scars left on the fossils it is important for the inferences to be clear for the results of any

332   modelling attempts.

333   While the ankle joint would be utilised at some stage in all the hypothesised take-offs,

334   our model was not able to reconstruct this joint with precision due to the missing model bones in

335   the reference specimen. Attempting muscle reconstruction without accurate models of the

336   missing bones would result in substantial error from uncertainty in the origin and insertion points

337   of the muscles (Meilak et al., 2021a). Other studies that have examined the moments produced

338   around the ankle in crocodilians and birds (Meilak et al., 2021a,b; Wiseman et al., 2021). As

339   both crocodilians and pterosaurs are plantigrade (Mazin et al., 2003; Mazin & Pouech, 2020), and

340   lack the tibiotarsus seen in birds, a crocodilian ankle mechanics approach may be a closer

341   approximation if the ankle muscles were to be estimated. These studies found the moments

342   produced by crocodiles to peak at be around half the peak moment of the knee (Wiseman et al.,

343   2021) while birds tended to peak at moment values equal or greater than the knee (Meilak et al.,

344   2021a,b). If such results are applied to pterosaurs, it is unlikely for either of the bipedal take-off

345   motions reach an equivalent amount of leverage as the quadrupedal launch motion.

346   When proposing a quadrupedal take-off, Habib (2008) determined that the forelimbs of

347   pterosaurs are stronger than the hindlimbs and as a result were likely able to withstand loads

348   associated with quadrupedal launch. Our results further support this finding by determining that

349   the muscle moment arms of the forelimb would be able to exert are also larger than the

350   hindlimb, allowing pterosaurs to utilise the greater force resistance highlighted by Habib (2008).

351   Our own prior research into pterosaur range of motion found that ornithocheiraean pterosaurs

352   can assume the poses required to quadrupedally take-off even when constrained by soft tissues

353   (Griffin et al., 2022). The OpenSim model results indirectly lend support to the water take-off

354   findings of Pittman et al. (2022) by highlighting the leverage possible in both the fore and

355   hindlimbs which could be used to power water take-offs. These results are contrary to the

356   findings presented by Padian *et al.* (2021) however that study focuses on a different pterosaur

357   morphology, that of the giant azhdarchids. This previous study also highlighted the lack of

358   moment arm analyses for the different launch hypotheses and raised concerns regarding the

359   use of bats as models for quadrupedal take-offs due to the lack of hindlimb use by bats. This

360   study addresses the moment arm concerns by determining that the moment arms of three

361   different pterosaur take-off kinematics and found the launch leverage to be available is greatest

362   when utilising the quadrupedal take-off motion (Figure 3C). Due to the lack of other recorded

363   quadrupedally launching modern fliers from which to compare and derive timings, bat-based

364   timing for the modelling of take-off in pterosaurs remains unavoidable though we have also

365   expanded the bat timing to incorporated hindlimb kinematics into the pterosaur take-off models.

366   Future work may be able to refine the kinematics and better address this concern, potentially

367   through forward kinematic approaches or iterative optimisation of reverse kinematic approaches

368   (Bishop et al., 2021).

369   A large moment arm does not inherently result in the creation of a larger force than

370   shorter moment arms as an increased muscle mass can offset the effect of shorter moment

371   arms. To get a better understanding of the overall moments generated by these kinematic

372   sequences further work is also needed to apply muscular force estimations to the moment arms

373   calculated for the pterosaur. The inclusion of muscular force estimations would also account for

374   potential mismatches between the implied force available with greater leverage and the effects

375   of muscle size. Additionally, the methods utilised in this study also need to be applied to the

376   azhdarchid and non-pterodactyloid pterosaur morphologies to better facilitate comparison and

377   develop a more complete understanding of pterosaur take-off.

378

379 **Acknowledgements**

383   Competing Interests

384   We have no conflicts of interest to declare.

385   Author Contributions

386   All authors contributed to writing the manuscript. BG co-designed the study, collected

387   the data, created the models, and ran the analyses. EMS co-designed the study, supplied the

388   original fossil material scans and model, sense-checked the soft tissue reconstructions and

389   supervised the project. EM created the OpenSim model creation pipeline and assisted with

390   model creation. RP sense-checked the soft tissue reconstructions. FC sense-checked the soft

391   tissue reconstructions. CP co-designed the study and supervised the project. ER co-designed

392   the study and supervised the project.

393

References

394   Ahrens J, Geveci B, Law C. 2004. ParaView: an End-UserTool for Large Data Visualization. In: Hansen CD,
396   Johnson CR eds. *Visualisation Handbook*. Elsevier,.

397   Alexander RM. 1998. All-time giants: the largest animals and their problems. *Palaeontology* 41:1231–
398   1245.

399   Allen VR, Kilbourne BM, Hutchinson JR. 2021. The evolution of pelvic limb muscle moment arms in bird-
400   line archosaurs. *Science Advances* 7. DOI: 10.1126/sciadv.abe2778.

401   An KN, Takahashi K, Harrigan TP, Chao EY. 1984. Determination of muscle orientations and moment
402   arms. *Journal of Biomechanical Engineering* 106:280–282. DOI: 10.1115/1.3138494.

403   Baron MG. 2021. The origin of Pterosaurs. *Earth-Science Reviews* 221. DOI:
404   10.1016/j.earscirev.2021.103777.

405   Bates KT, Maidment SCR, Allen VR, Barrett PM. 2012. Computational modelling of locomotor muscle
406   moment arms in the basal dinosaur Lesothosaurus diagnosticus: Assessing convergence between
407   birds and basal ornithischians. *Journal of Anatomy* 220:212–232. DOI: 10.1111/j.1469-
408   7580.2011.01469.x.

409   Bennett SC. 2001a. The Osteology and Functional Morphology of the Late Cretaceous Pterosaur
410   *Pteranodon* Part II. Size and Functional Morphology. *Palaeontographica, Abteilung A:*
411   *Palaozoologie - Stratigraphie* 260:113–153.

412   Bennett SC. 2001b. The Osteology and Functional Morphology of the Late Cretaceous Pterosaur
413   *Pteranodon*: Part I. General Description of Osteology. *Palaeontographica, Abteilung A:*
414   *Palaozoologie - Stratigraphie* 260:113–153.

415   Bennett SC. 2003. Morphological evolution of the pectoral girdle of pterosaurs: myology and function.
416   *Geological Society, London, Special Publications* 217:191–215. DOI:
417   10.1144/GSL.SP.2003.217.01.12.

418   Bennett SC. 2008. Morphological evolution of the wing of pterosaurs: Myology and function. *Zitteliana*
419   *Reihe B: Abhandlungen der Bayerischen Staatssammlung fur Palaontologie und Geologie*:127–141.

420   Bishop PJ, Cuff AR, Hutchinson JR. 2021. How to build a dinosaur: Musculoskeletal modeling and
421   simulation of locomotor biomechanics in extinct animals. *Paleobiology* 47:1–38. DOI:
422   10.1017/pab.2020.46.

423   Bishop PJ, Falisse A, De Groote F, Hutchinson JR. 2021. Predictive Simulations of Musculoskeletal
424   Function and Jumping Performance in a Generalized Bird. *Integrative Organismal Biology* 3. DOI:
425   10.1093/iob/obab006.

426   Bramwell CD, Whitfield GR. 1974. Biomechanics of Pteranodon. *Philosophical Transactions of the Royal*
427   *Society B: Biological Science* 267:503–581.

428   Chatterjee S, Templin RJ. 2004. Posture, locomotion, and paleoecology of pterosaurs. *Geological Society*
429   *of America Special Publication* 376:1–64. DOI: 10.1130/0-8137-2376-0.1.

430 Chatterjee S, Templin RJ. 2012. The Flight Dynamics of Tapejara, a Pterosaur From the Early Cretaceous
431   of Brazil with a Large Cranial Crest. *Acta Geologica Sinica - English Edition* 86:1377–1388. DOI:
432   10.1007/s00192-011-1546-5.

433 Costa FR, Rocha-Barbosa O, Kellner AWA. 2014. Myological reconstruction of the pelvic girdle of
434   Anhanguera piscator (Pterosauria: Pterodactyloidea) using three dimensional virtual animation.
435   *Revista Brasileira de Paleontologia* 17:11–22. DOI: 10.4072/rbp.2014.1.02.

436 Delp SL, Loan JP. 2000. A computational framework for simulating and analyzing human and animal
437   movement. *Computing in Science and Engineering* 2. DOI: 10.1109/5992.877394.

438 Dilkes DW. 1999. Appendicular myology of the hadrosaurian dinosaur *Maiasaura peeblesorum* from the
439   Late Cretaceous (Campanian) of Montana. *Transactions of the Royal Society of Edinburgh: Earth
440   Sciences* 90:87–125. DOI: 10.1017/S0263593300007185.

441 Earls K. 2000. Kinematics and Mechanisms of Ground Take-off in the Startling *Sturnis Vulgaris* and the
442   Quail *Coturnix Coturnix*. *Journal of Experimental Biology* 203:725–739. DOI:
443   10.1523/JNEUROSCI.2773-10.2010.

444 Ezcurra MD, Nesbitt SJ, Bronzati M, Dalla Vecchia FM, Agnolin FL, Benson RBJ, Brissón Egli F, Cabreira SF,
445   Evers SW, Gentil AR, Irmis RB, Martinelli AG, Novas FE, Roberto da Silva L, Smith ND, Stocker MR,
446   Turner AH, Langer MC. 2020. Enigmatic dinosaur precursors bridge the gap to the origin of
447   Pterosauria. *Nature* 588:445–449. DOI: 10.1038/s41586-020-3011-4.

448 Fastnacht M. 2005. The first dsungaripterid pterosaur from the Kimmeridgian of Germany and the
449   biomechanics of pterosaur long bones. *Acta Palaeontologica Polonica* 50:273–288.

450 Foffa D, Dunne EM, Nesbitt SJ, Butler RJ, Fraser NC, Brusatte SL, Farnsworth A, Lunt DJ, Valdes PJ, Walsh
451   S, Barrett PM. 2022. Scleromochlus and the early evolution of Pterosauromorpha. *Nature* 610:313–
452   318. DOI: 10.1038/s41586-022-05284-x.

453 Frigot RA. 2017. Pelvic musculature of Vectidraco daisymorrisae and consequences for pterosaur
454   locomotion. *Geological Society of London Special Publication* 455:45–55. DOI:
455   10.1016/j.matlet.2011.05.028.

456 Goto Y, Yoda K, Weimerskirch H, Sato K. 2022. How did extinct giant birds and pterosaurs fly? A
457   comprehensive modeling approach to evaluate soaring performance. *PNAS Nexus*:1–16. DOI:
458   10.1093/pnasnexus/pgac023.

459 Griffin B, Martin-Silverstone E, Demuth O, Pêgas R, Palmer C, Rayfield E. 2022. Constraining pterosaur
460   launch: range of motion in the pectoral and pelvic girdles of a medium-sized ornithocheiraean
461   pterosaur. *Biological Journal of the Linnean Society*. DOI: 10.1093/biolinnean/blac063.

462 Habib MB. 2008. Comparative evidence for quadrupedal launch in pterosaurs. *Zitteliana* B28:159–166.

463 Henderson DM. 2010. Pterosaur body mass estimates from three-dimensional mathematical slicing.
464   *Journal of Vertebrate Paleontology* 30:768–785. DOI: 10.1080/02724631003758334.

465   Hone DWE, Van Rooijen MK, Habib MB. 2015. The wingtips of the pterosaurs: Anatomy, aeronautical
466   function and ecological implications. *Palaeogeography, Palaeoclimatology, Palaeoecology*
467   440:431–439. DOI: 10.1016/j.palaeo.2015.08.046.

468   Hutchinson JR, Anderson FC, Blemker SS, Delp SL. 2005. Paleontological Society Analysis of Hindlimb
469   Muscle Moment Arms in Tyrannosaurus rex Using a Three- Dimensional Musculoskeletal Computer
470   Model : Implications for Stance , Gait , and Speed Author (s): John R . Hutchinson , Frank C .
471   Anderson , Silvia S . *Paleobiology* 31:676–701.

472   Hutchinson JR, Rankin JW, Rubenson J, Rosenbluth KH, Siston RA, Delp SL. 2015. Musculoskeletal
473   modelling of an ostrich (*Struthio camelus*) pelvic limb: Influence of limb orientation onmuscular
474   capacity during locomotion. *PeerJ* 2015:1–52. DOI: 10.7717/peerj.1001.

475   Kambic RE, Roberts TJ, Gatesy SM. 2014. Long-axis rotation: A missing degree of freedom in avian
476   bipedal locomotion. *Journal of Experimental Biology* 217:2770–2782. DOI: 10.1242/jeb.101428.

477   Kellner AWA, Holgado B, Grillo O, Pretto FA, Kerber L, Pinheiro FL, Soares MB, Schultz CL, Lopes RT,
478   Araújo O, Müller RT. 2022. Reassessment of Faxinalipterus minimus, a purported Triassic pterosaur
479   from southern Brazil with the description of a new taxon. *PeerJ* 10. DOI: 10.7717/peerj.13276.

480   Maidment SCR, Bates KT, Barrett PM. 2014. modeling of pelvic locomotor muscle moment arms in
481   Edmontosaurus. *Hadrosaurs*.

482   Martin-Silverstone E. 2017. Insights into mass estimation, pneumaticity, and anatomy of pterosaurs:
483   implications for locomotion. Doctor of Philosophy Thesis. University of Southampton.

484   Martin-Silverstone E, Sykes D, Naish D. 2018. Does postcranial palaeoneurology provide insight into
485   pterosaur behaviour and lifestyle? New data from the azhdarchoid *Vectidraco* and the
486   ornithocheirids *Coloborhynchus* and *Anhanguera*. *Palaeontology* 62:197–210. DOI:
487   10.1111/pala.12390.

488   Mazin JM, Billon-Bruyat J-P, Hantzepergue P, Larauire G. 2003. Ichnological evidence for quadrupedal
489   locomotion in pterodactyloid pterosaurs: Trackwaysfrom the Late Jurassic of Crayssac. In: *Evolution*
490   *and Palaeobiology of Pterosaurs*. 283–296.

491   Mazin JM, Pouech J. 2020. The first non-pterodactyloid pterosaurian trackways and the terrestrial ability
492   of non-pterodactyloid pterosaurs. *Geobios* 58:39–53. DOI: 10.1016/j.geobios.2019.12.002.

493   Meilak EA, Gostling NJ, Palmer C, Heller MO. 2021a. On the 3D Nature of the Magpie (Aves: Pica pica)
494   Functional Hindlimb Anatomy During the Take-Off Jump. *Frontiers in Bioengineering and*
495   *Biotechnology* 9. DOI: 10.3389/fbioe.2021.676894.

496   Meilak EA, Provini P, Palmer C, Gostling NJ, Heller MO. 2021b. On the hindlimb biomechanics of the
497   avian take-off leap. *bioRxiv preprint*. DOI: 10.1101/2021.11.19.469279.

498   Modenese L, Kohout J. 2020. Automated Generation of Three-Dimensional Complex Muscle Geometries
499   for Use in Personalised Musculoskeletal Models. *Annals of Biomedical Engineering* 48:1793–1804.
500   DOI: 10.1007/s10439-020-02490-4.

501   Molnar J. 2009. How giant reptiles flew: visualizing quadrupedal launch in pterosaurs. Master's Thesis
502   Thesis. Johns Hopkins University.

503   Padian K. 1983. A Functional Analysis of Flying and Walking in Pterosaurs. *Paleobiology* 9:218–239. DOI:
504   10.1042/BST20150065.

505   Padian K, Cunningham JR, Langston W, Conway J. 2021. Functional morphology of *Quetzalcoatlus*
506   Lawson 1975 (Pterodactyloidea: Azhdarchoidea). *Journal of Vertebrate Paleontology* 41:218–251.
507   DOI: 10.1080/02724634.2020.1780247.

508   Pandy MG. 1999. Moment Arm of a Muscle Force. *Exercise and Sport Science Reviews* 27:79–118.

509   Pennycuick CJ. 1968. Power requirements for horizontal flight in the pigeon *Columba livia*. *Journal of*
510   *Experimental Biology* 49:527–555.

511   Pittman M, Kaye TG, Campos HBN, Habib MB. 2022. Quadrupedal water launch capability demonstrated
512   in small Late Jurassic pterosaurs. *Scientific Reports* 12:1–8. DOI: 10.1038/s41598-022-10507-2.

513   Rayner JM V. 1988. Form and Function in Avian Flight. *Current Ornithology* 5:1–66. DOI: 10.1007/978-1-
514   4615-6787-5_1.

515   Rayner JM V. 1989. Mechanics and physiology of flight in fossil vertebrates. *Transactions of the Royal*
516   *Society of Edinburgh: Earth Sciences* 80:311–320.

517   Schutt Jr. WA, Scott Altenbach J, Chang YHH, Cullinane DMM, Hermanson JW, Muradali F, Bertram JEAE.
518   1997. The dynamics of flight-initiating jumps in the common vampire bat Desmodus rotundus. *The*
519   *Journal of experimental biology* 200:3003–12. DOI: citeulike-article-id:418833.

520   Seth A, Hicks JL, Uchida TK, Habib A, Dembia CL, Dunne JJ, Ong CF, DeMers MS, Rajagopal A, Millard M,
521   Hamner SR, Arnold EM, Yong JR, Lakshmikanth SK, Sherman MA, Ku JP, Delp SL. 2018. OpenSim:
522   Simulating musculoskeletal dynamics and neuromuscular control to study human and animal
523   movement. *PLOS Computational Biology* 14:e1006223. DOI: 10.1371/journal.pcbi.1006223.

524   Sherman MA, Seth A, Delp SL. 2013. What is a moment arm? Calculating muscle effectiveness in
525   biomechanical models using generalized coordinates. In: *Proceedings of the ASME 2013*
526   *International Design Engineering Technical Conferences and Computers and Information in*
527   *Engineering Conference*. 1–9.

528   Tokita M. 2015. How the pterosaur got its wings. *Biological Reviews* 90:1163–1178. DOI:
529   10.1111/brv.12150.

530   Wiseman ALA, Bishop PJ, Demuth OE, Cuff AR, Michel KB, Hutchinson JR. 2021. Musculoskeletal
531   modelling of the Nile crocodile (Crocodylus niloticus) hindlimb: Effects of limb posture on leverage
532   during terrestrial locomotion. *Journal of Anatomy* 239:424–444. DOI: 10.1111/joa.13431.

533   Witmer LM. 1995. The Extant Phylogenetic Bracket and the importance of reconstructing soft tissues in
534   fossils. In: Thompson J ed. *Functional Morphology in Vertebrate Paleontology*. New York, New
535   York: Cambridge University Press, 19–33.

536   Witton MP. 2008. A new approach to determining pterosaur body mass and its implications for
537   pterosaur flight. *Zitteliana* B28:143–159.

538   Witton MP. 2013. *Pterosaurs Natural History, Evolution, Anatomy*. Princeton, USA: Princeton University
539   Press.

540   Witton MP, Habib MB. 2010. On the size and flight diversity of giant pterosaurs, the use of birds as
541   pterosaur analogues and comments on pterosaur flightlessness. *PLoS ONE* 5:e13982. DOI:
542   10.1371/journal.pone.0013982.

543

544

545   Software References

546   Geomagic Studio, 3Dsystems, Morrisville, NC, USA.

547   MATLAB version 2021a. Mathworks Inc., URL: uk.mathworks.com/products/matlab

548   Maya 2019. Autodesk, URL: www.autodesk.co.uk/products/maya

549   ParaView version 5.9.0-RC3. Kitware, URL: www.paraview.org

550   R Core Team (2021). R: A language and environment for statistical computing. R Foundation for

551   Statistical Computing, Vienna, Austria. Version 4.1.2 URL https://www.R-project.org/.

552   Supplementary summary:

553   Supplemental tables and figures included in separate document.

554   Supplemental Excel Workbook: Extended muscle reconstruction workbook available upon

555   request and will be uploaded to data.bris online repository (with DOI) on final publication.

556   Zip folder "MMA" contains all raw output data from OpenSim and subsequent randomisations.

557   This will also be included in the data.bris DOI.

558   Model Availability: 3D models of some of the skeletal elements are associated with previous

559   papers (Martin-Silverstone, Sykes & Naish, 2018; Griffin et al., 2022). The complete OpenSim model

560   and movement files will be uploaded to the data.bris repository and the OpenSim website where

561   it will be freely available to download on publication.

Table 1 (on next page)

Modelled muscle tendon units (MTUs) for the OpenSim Ornithocheiraean model.

* indicates MTUs not directly related to the take-offs. Muscles using averaged MTUs include the number of MTUs used in the origin and insertion columns.

code	Muscle	Origin	Inference	Insertion	Inference
		Pectoral group			
SCM*	sternocleidomastoideus	anterior sternum	I	squamosal	I'
SC*	sternocoracoideus	anterior margin of sternum	II'	coracoid	II
LD	latissimus dorsi	last cervical neural spine to distal notarium – 3 MTUs	I'	dorsal (distal) humerus shaft scar	I
TM	teres major	posterolateral scapula	II	dorsal (proximal) humerus shaft scar	II
DS	deltoides scapularis	lateral scapula/acromion process	I	dorsal (anterior) deltopectoral crest	I'
SHA	scapulohumeralis anterior	scapula anterior to glenoid	II	dorsal (proximal) deltopectoral crest	II'
SHP	scapulohumeralis posterior	posterior margin scapula above glenoid	I	dorsal posterior process of humerus distal to SUBS	I
SUBS	subscapularis	medial ventral surface scapula	I	dorsal posterior process of humerus	I
TR-S	triceps	scapula - dorsal border of glenoid	I	olecranon process ulna	I
TR-C	triceps	coracoid - ventral posterior to glenoid	II'	olecranon process ulna	II
TR-M	triceps	medial - posterior side humeral shaft	I	olecranon process ulna	I
TR-L	triceps	lateral - anterior side humeral shaft	II	olecranon process ulna	II
PECT	Pectoralis	sternum ventral – 4 MTUs	I	entire ventral deltopectoral crest	I
SUPC	supracoracoideus	anterior ventral surface of coracoid	II	ventral proximal to deltopectoral crest	II'
CB	Coracobrachialis	posterior ventral coracoid – 3 MTUs	I	ventral posterior to deltopectoral crest	I
BI	Biceps	coracoid biceps tubercule	I	proximal radius/ulna – 2 MTUs	I
BR	brachialis	anterior humerus shaft	I'	proximal radius/ulna	I
HR	humeroradialis	proximal humerus distal to CB	II'	proximal radius	II'

|					
FDL	flexor digitorum longus (quarti)	medial epicondyle of humerus and ulna	II	ventral extensor process WP1 and distal phalanges	I'
FDL-U	flexor digitorum longus (quarti)	medial ulna shaft Ulna	I	ventral extensor process WP1 and distal phalanges	I'
EDL	extensor digitorum longus (quarti)	lateral epicondyle of humerus	I	proximal posterior WP1 process	I'
FCU	flexor carpi ulnaris	medial epicondyle of humerus	I	anterior proximal WMC	II'
FCR	flexor carpi radialis	medial epicondyle of humerus	I	Proximal anterior syncarpal	II
ECU	extensor carpi ulnaris	lateral epicondyle of humerus	I	posterior WMC large scar	II
ECR	extensor carpi radialis	lateral epicondyle of humerus	I	Proximal posterior syncarpal	II'
SUP	supinator	ridge anterior to lateral epicondyle of humerus	I	¾ length of posterior radius shaft	I
PT	pronator teres	medial epicondyle of humerus	I	posterior mid shaft	I
PQ	pronator quadratus	ulna shaft	I	posterior distal radius shaft	I
FDB	flexor digitorum brevis	dorsal distal syncarpal	II'	dorsal extensor process WP1	I
EDB	extensor digitorum brevis	ventral distal syncarpal	II'	posterior WP1 process	II
Pelvic Group					
ADD	adductor femoris	lateral surface of the ischium	I	medial shaft (diaphysis) of the femur	I
IFM	illiofemoralis	Lateral margin of preacetabular process of the ilium	I	greater trochanter	I
PIFE	puboischiofemoralis externus	Lateral surface of the pubis	I	greater trochanter	I
PIFI	puboischiofemoralis internus	medial surface of ilium anterior to acetabulum	I	proximal surface of femur	I
AMB	ambiens	pubic tubercule	I	cnemial crest of tibia	I'
ITB	Iliotibialis	Lateral margin of preacetabular process of the ilium – 3 MTUs	I	cnemial crest of tibia	I'
FTE	flexor tibialis externus	lateral surface of the postacetabular process of the ilium	II	medial surface of the tibia	II'
FTI-I	flexor tibialis internus	lateral surface of ischial tuberosity – 2 MTUs	II	posteromedial shaft of tibia	II'

FTI-II	flexor tibialis internus 2	lateral surface of the postacetabular process of the ilium	II	posteromedial shaft of tibia	II'
ILF	iliofibularis	lateral surface of the postacetabular process of the ilium	II'	posteromedial shaft of tibia	II'
CFB	caudofemoralis brevis	lateral iliac surface	I'	posterior (4th) trochanter of femur	I
FMTE	femorotibialis externus	proximal femoral shaft	I	cnemial crest of tibia	I'
FMTI	femorotibialis internus	proximal femoral shaft	I	cnemial crest of tibia	I'

1

Figure 1

Musculoskeletal model used in this study with labelled MTUs and joints in A) lateral, B) posterior and C) anterior views.

Muscle abbreviations follow the codes set forth in Table 1.
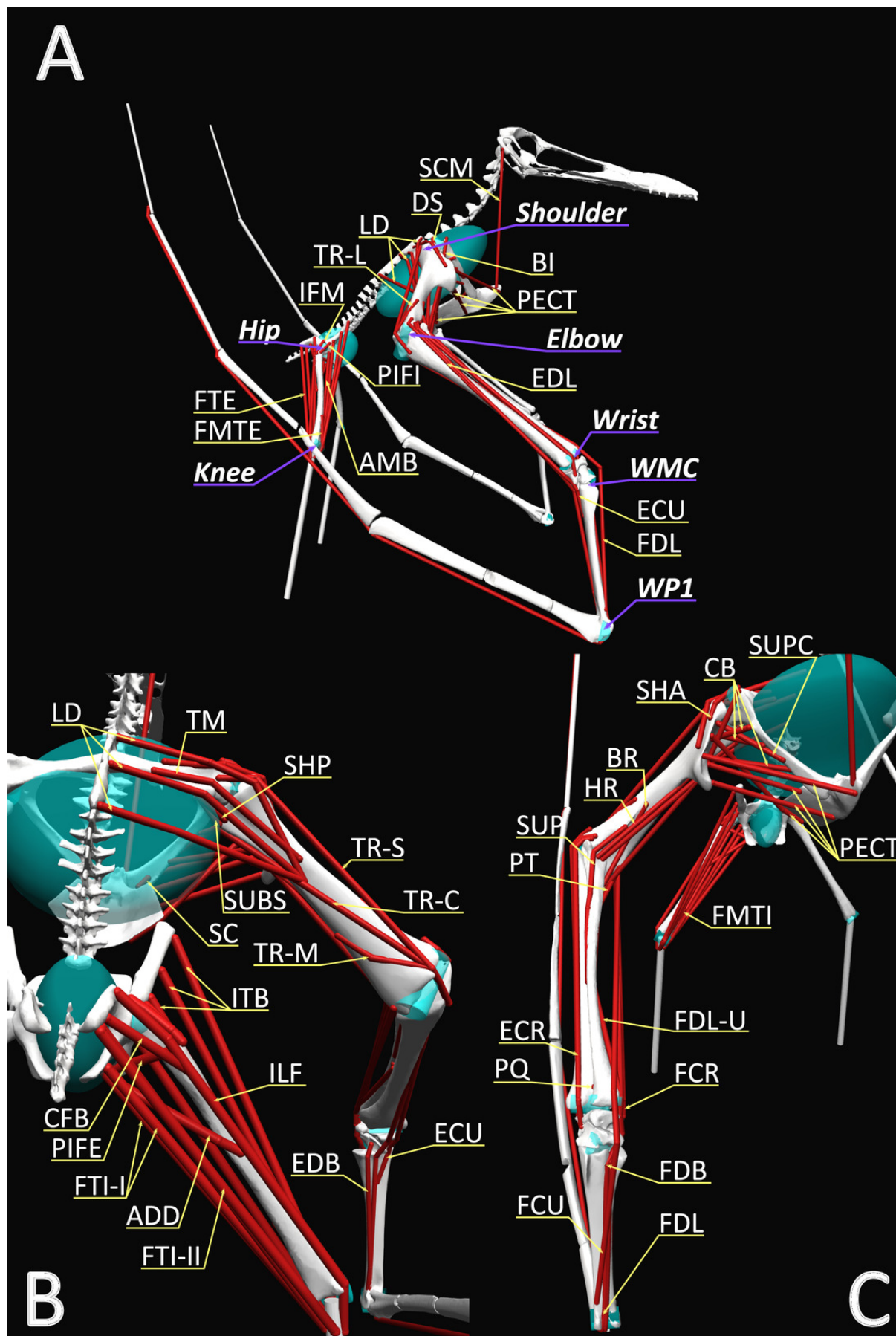
Figure 2

Simplified pterosaur model showing the directionality of the joint degrees of freedom examined in this study

Solid arrows show the direction of positive rotation while the dashed arrows indicate the resultant movement of the element. Colours follow standard 3D space axes with positive X axis rotation controlling long axis rotation (pronation, red), positive Y axis rotation controlling extension (green), and positive Z axis rotation controlling adduction (blue). A colour sensitive variant has been included in the supplementary material (Figure S8).

Hip

Shoulder

Knee

Elbow

WMC

WP1
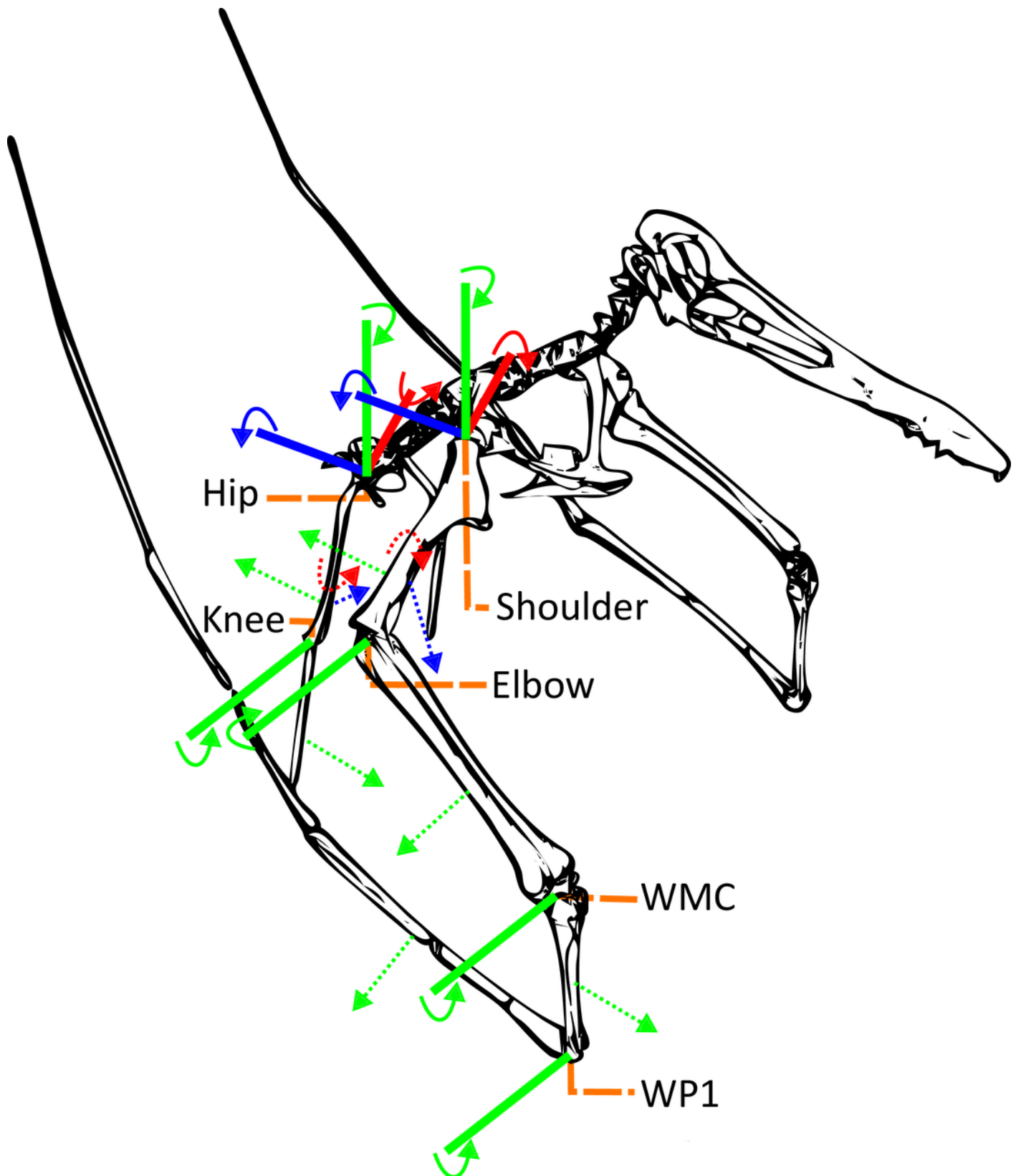
Figure 3

One second take-off sequences used in this study highlighting key phases.

A) Bipedal burst style take-off with crouched, ankle lifted, and launch phase timings highlighted. B) Bipedal countermotion style take-off with countermotion and launch phase timings highlighted. C) Quadrupedal take-off style with crouch, vault, and launch phases highlighted.
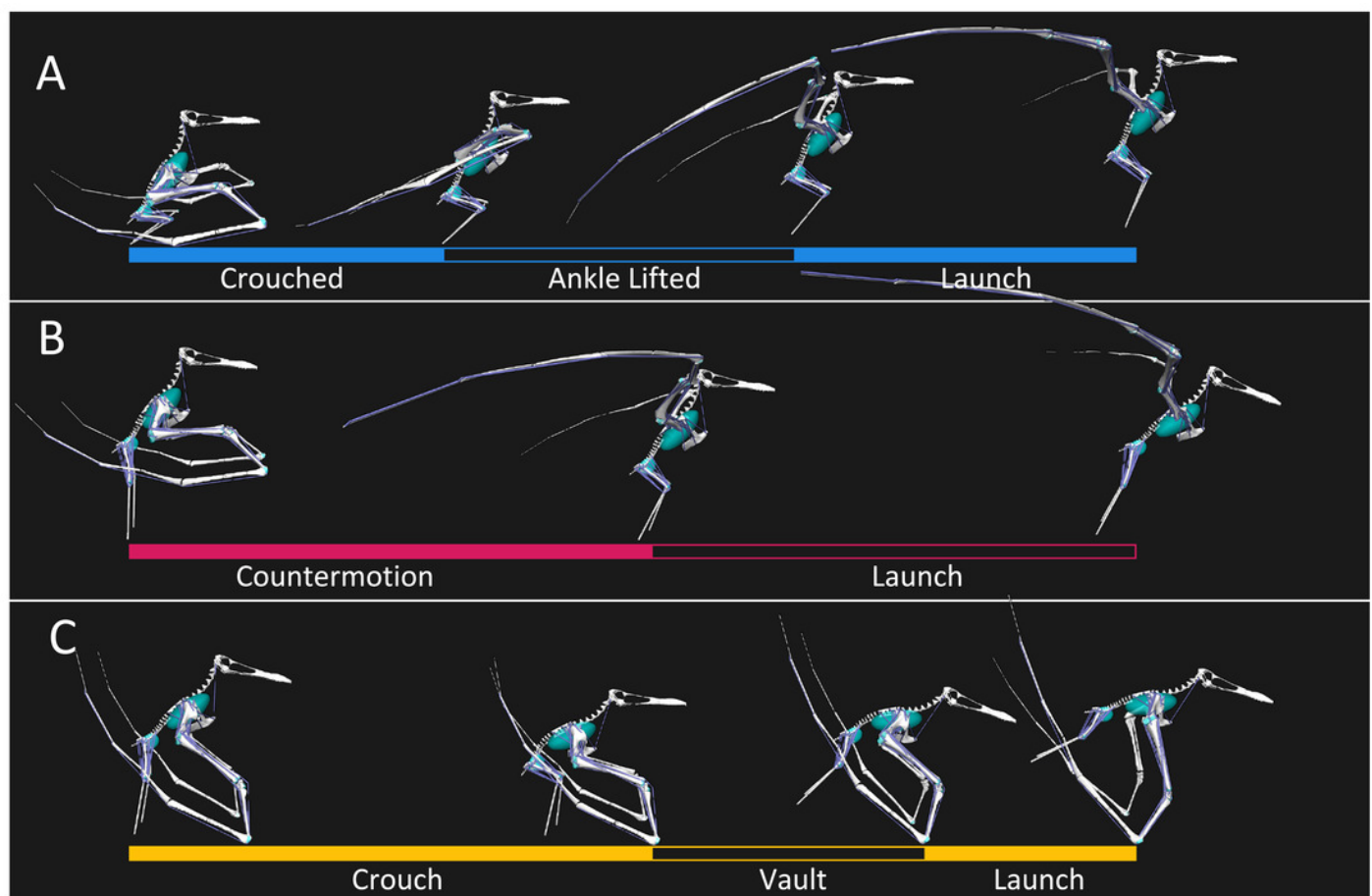
Figure 4

Summed moment arms in each hypothesised take-off motion for the shoulder and elbow rotational DOFs.
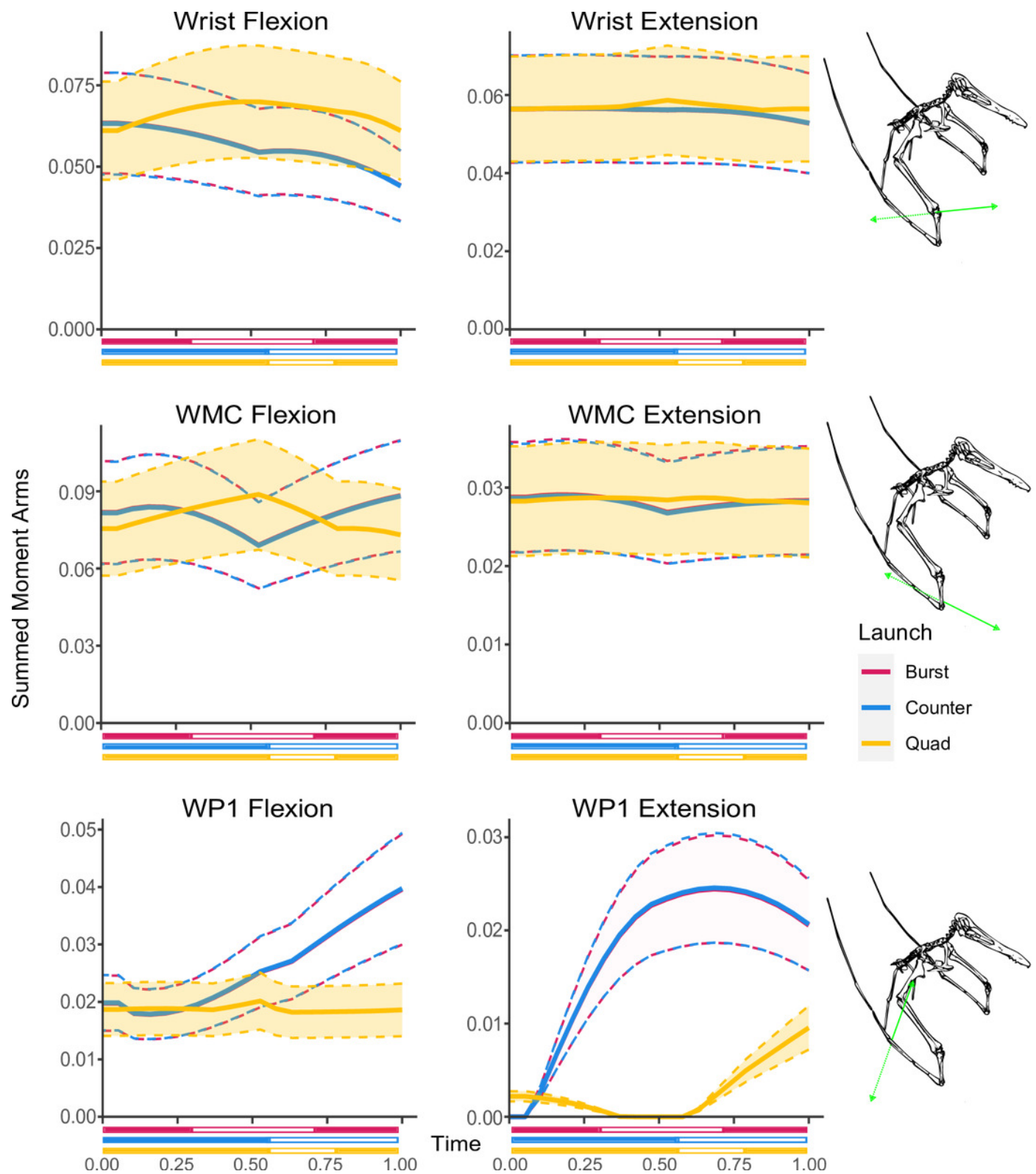
Solid lines indicate mean values following Monte Carlo simulation, dashed lines show estimated error, colouration indicates moment arm usage throughout the take-off. Take-off phase markers are equivalent to Figure 3.
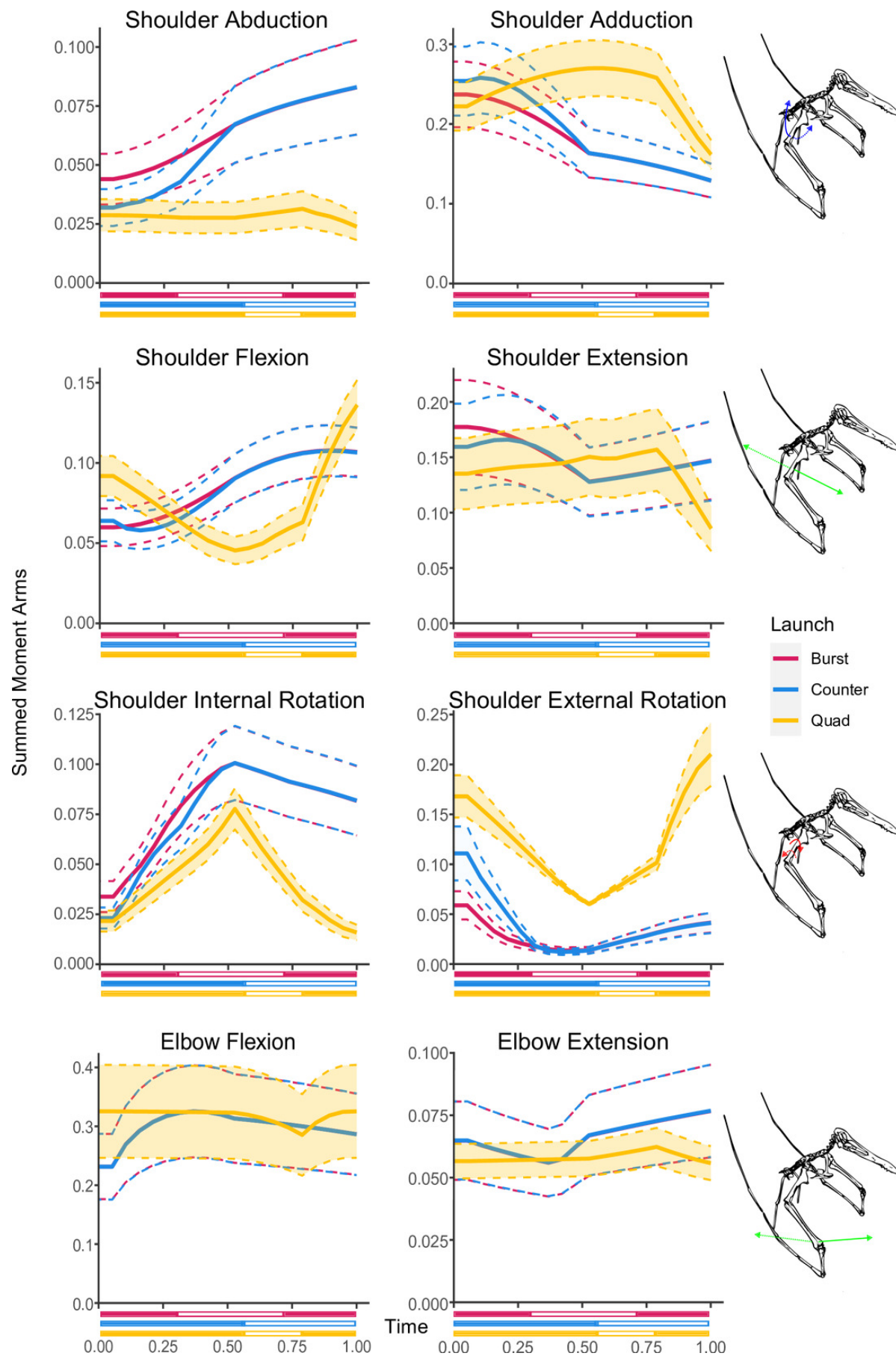
Figure 5

Summed moment arms in each hypothesised take-off motion for the lower forelimb rotational DOFs.

Solid lines indicate mean values following Monte Carlo simulation, dashed lines show estimated error, colouration indicates moment arm usage throughout the take-off. Take-off phase markers are equivalent to Figure 3.

Figure 6

Summed moment arms in each hypothesised take-off motion for the hindlimb rotational DOFs.

Solid lines indicate mean values following Monte Carlo simulation, dashed lines show estimated error, colouration indicates moment arm usage throughout the take-off. Take-off phase markers are equivalent to Figure 3.